Monovacancy formation energies and Fermi surface topological transitions in Pd-Ag alloys

E. K. Delczeg-Czirjak,[1,*] L. Delczeg,[2] L. Vitos,[1,3,4] and O. Eriksson[1]

[1]*Division of Materials Theory, Department of Physics and Astronomy, Uppsala University, Box 516, SE-751 20, Uppsala, Sweden*

[2]*Royal Institute of Technology (KTH), Stockholm, Sweden*

[3]*Applied Materials Physics, Department of Materials Science and Engineering, Royal Institute of Technology (KTH), SE-100 44 Stockholm, Sweden*

[4]*Research Institute for Solid State Physics and Optics, Wigner Research Center for Physics, P.O. Box 49, HU-1525 Budapest, Hungary*

(Received 5 May 2015; revised manuscript received 9 October 2015; published 10 December 2015)

Using first-principles mean-field alloy theory, we calculate the vacancy formation energies of the face-centered-cubic Pd-Ag alloys as a function of chemical composition. The effect of Fermi surface topological transition on the composition dependence of the vacancy formation energies is detectable and is consistent with what has previously been shown for the bulk properties of $Pd_{1-x}Ag_x$.

DOI: 10.1103/PhysRevB.92.224107 PACS number(s): 71.15.Nc, 61.72.jd, 71.20.Be, 81.05.Bx

I. INTRODUCTION

Palladium-silver alloys are important materials from a technological point of view. Besides the jewelry industry, they are used in dentistry as bridges and crowns due to their nobility and resistance to tarnishing [1,2]. These alloys are also ductile and have good electrical conductivity; therefore they are used in conductive films and pastes, multilayer capacitors, or as contacts. Palladium-silver nanoparticles and thin films are key components of biosensors [3] and chemical sensors [4], respectively. They also can be used as catalysts in chemical reactions [5]. The most recent application of the Pd-Ag alloys is as hydrogen separation membranes [6,7]. Hydrogen has a high potential to become an environmentally friendly energy carrier. Hydrogen is the most abundant element on the Earth, but due to its high reactivity, it can be found only in chemical compounds. Separation and purification of H from a multicomponent gas mixture may be realized using Pd-Ag membranes [6,7].

Palladium and silver form continuous solid solution within the face-centered-cubic (fcc) crystallographic phase [8] for the whole range of concentration according to the high-temperature experimental phase diagram [9]. Due to their simple crystal structure and complete miscibility, Pd-Ag alloys have been seen as prototype systems, where the electronic properties, and through this the physical properties, can be controllably altered. Therefore they become popular model systems for investigations at fundamental atomistic level. Charge transfer has been studied with x-ray-absorbtion near edge structures and x-ray photoemission spectroscopy [10], and recently, kinetic energy shifts with Auger spectroscopy [11]. Although Pd-Ag alloys are regarded as simple systems, their physical properties, for example lattice parameters [12], have complex behavior with gradually changing composition.

The above mentioned technological applications and the deviation from Vegard's law motivated several electronic structure calculations [13–30]. The successful reproduction of the experimental mixing enthalpy, Gibb's energy curves, and composition-dependent lattice parameters encouraged further theoretical work. Formation of low-temperature ordered structures has been predicted for different compositions [14,18]. Surface segregation [15,21,22] effects, surface core-level shift [23], surface stress [24] composition dependent elastic properties [25–27] and stacking fault energies [29], and short and long range ordering effects on the elastic properties [26,27] have been discussed in the past 20 years. The composition dependence of the experimentally measured and theoretically calculated physical parameters shows strong deviation from the linear rule of mixing. This strongly nonlinear composition dependence has been associated with Fermi surface topological transitions (FSTT's) [16,25,27,29]. Different pair-potential models [20,28] and Monte Carlo methods [31] have used Pd-Ag alloys as test systems to validate the applicability of the newly developed method.

The most common point defects in metallic crystalline systems are monovacancies. Although their concentration is small (10^{-3} to 10^{-4} in pure metals at the melting temperature [32]), they may affect drastically the transport and mechanical properties of metals. Their concentration and formation energy are the key quantities in the description of vacancy-related properties. Due to the large change of the electronic density for atoms around the vacancy, the vacancy formation energy calculations often have been used to test the performance of different exchange-correlation functionals [33–39] as well as different density functional theory methods [40–42]. A well established theoretical tool may be helpful in determination of the vacancy formation energies for materials where the experimental measurements face difficulties [32].

In the present work we discuss the vacancy formation energies as a function of composition. Results are calculated using three different exchange-correlation functionals. A nonlinear composition dependence is identified for vacancy formation energies similarly to the above mentioned physical parameters. Here we show that the formation energy of this particular crystal defect is also affected by the FSTT. The paper is divided as follows: Sec. II briefly describes the employed theoretical approach, and the results are presented in Sec. III. Discussion and conclusion of the disclosed results are included in Secs. IV and V.

II. METHODOLOGY

We adopt the supercell technique to calculate vacancy formation energies (H_{vac}). A $2 \times 2 \times 2$ supercell (SC) was

*erna.delczeg@physics.uu.se

built up from the conventional fcc unit cell. The SC finally has simple cubic symmetry with 32 sites per primitive cell from which one site is substituted by a vacancy corresponding to 1/32 vacancy concentration in the homogeneous bulk alloy. The volume-relaxed vacancy formation energy ($H_{\rm vr}$) was obtained by means of $H^N_{\rm vr}(0) = E^N_{\rm SC}(0) - (N-1)E_0$ where $E_{\rm SC}(0)$ is the total energy of the SC at its equilibrium volume, E_0 represents the total energy of the fcc unit cell at the bulk equilibrium volume, and N is the number of sites in the SC. In the present case $N = 32$. Experiments show a distortion of the lattice around the vacancy. For a more realistic geometry around the vacancy, we included in the present study the local lattice relaxation by computing the total energy of the supercell [$E_{\rm SC}(\eta)$] as a function of the distance $d = (1+\eta)d_0$ between the vacancy and the 12 atomic sites from the first coordination shell around the vacancy. Here, d_0 is the ideal unrelaxed nearest-neighbor distance in the fcc lattice. The fully relaxed vacancy formation energy ($H_{\rm fr}$) is obtained from the minimum of the formation energy $H^N_{\rm fr}(\eta) = E^N_{\rm SC}(\eta) - (N-1)E_0$, viz., $H^N_{\rm fr} = \min_\eta H^N_{\rm fr}(\eta) = H^N_{\rm fr}(\eta_0)$, where η_0 the equilibrium local relaxation around the vacancy. This type of local relaxation within the present mean-field approximation is motivated by former results which have shown that the size of the local relaxation is quite similar in different metals [37] and it has been successfully applied for paramagnetic austenitic Fe-Cr-Ni alloys [43].

Total energy calculations were carried out using density functional theory [44,45] formulated within the exact muffin-tin orbital (EMTO) method [42,46–48] in combination with the full charge density technique [49] and the mean-field coherent-potential approximation (CPA) [50,51]. The latter is used to treat the chemical disorder between Pd and Ag. For a full description of the EMTO method the reader is referred to Ref. [42]. The EMTO basis set included s, p, d, and f orbitals for bulk and supercell calculations. The one-electron equations were solved within the soft-core and scalar-relativistic approximations. The Green's function was calculated for 16 complex energy points distributed exponentially on a semicircular contour including states within 1 Ry below the Fermi level. For the one-center expansion of the full charge density $l^h_{\rm max} = 8$ cutoff was used. The electrostatic correction to the single-site coherent potential approximation was described using the screened impurity model [52] with a screening parameter of 0.9. Total energies were calculated using three different exchange-correlation functionals (xcf's): the local density approximation (LDA) [53], the AM05 approximation [35], and the revised version of the Perdew-Burke-Ernzerhof exchange correlation approximation for solids and surfaces (PBEsol) [54]. For the local lattice relaxation around the vacancy, we used both compressed ($\eta = -6, -4, -2$ %) and expanded ($\eta = 2$%) nearest-neighbor distances. The minimum of $E_{\rm SC}(\eta)$ was obtained from a second-order polynomial fit. The k-space sampling was performed with a uniform k mesh within the Brillouin zone. The number of k points was established (see Ref. [37]) such that the numerical error of $H_{\rm vac}$ is below 0.01 eV. For the Fermi surface calculations, 27 000 k points was used within the fcc unit cell. Previous theoretical works have shown that a 32-atom SC is large enough for accurate calculation of the vacancy formation energy in some selected metals [41,46,55,56]. A similar test on the finite-size effect on the volume-relaxed vacancy formation energy was performed here using a $3\times3\times3$ SC containing 108 atoms. $H_{\rm vr}$ calculated within a $3\times3\times3$ SC is found to be lower with 0.03 (0.12) eV for Pd (Ag) than data obtained in a $2\times2\times2$ SC. The error bar of the theoretical data is set to 0.075 eV. The effect of the electronic temperature on the volume-relaxed formation energy of Pd is 0.02 eV at 500 K. This is below the error bar established above; therefore further calculations were performed at 0 K without taking into account the finite-temperature Fermi-Dirac distribution.

III. RESULTS

A. Bulk parameters of Pd and Ag

The accuracy of the EMTO method is assessed by comparing the present results for Pd and Ag with the previous theoretical and available experimental data. Bulk parameters (bulk modulus B and lattice parameter a) volume-relaxed ($H_{\rm vr}$) and fully relaxed ($H_{\rm fr}$) vacancy formation energies calculated with the EMTO method for pure Pd and Ag are listed in Table I together with the available experimental and former theoretical results.

Lattice parameters obtained using EMTO are in very good agreement compared with the data calculated using the

TABLE I. Lattice parameters (a in units of Å), bulk modulus (B in units of GPa), volume ($H_{\rm vr}$), and fully relaxed ($H_{\rm fr}$) vacancy formation energies (in units of eV) for bulk fcc Pd and Ag in comparison with the available experimental and former theoretical data. The literature data are taken from Refs. [34] [a], [38] [b], [41] [c], [40] [d], [57] [e], [58] [f], [59] [g], [32] [h], and [60] [i]. Recommended experimental value for Ag is highlighted by boldface.

	Method	$a^{\rm fcc}$	$B^{\rm fcc}$	$H_{\rm vr}$	$H_{\rm fr}$
Pd	EMTO-LDA	3.854	223	1.72	1.48
	EMTO-AM05	3.884	199	1.72	1.50
	EMTO-PBE	3.956	165	1.38	1.21
	EMTO-PBEsol	3.889	205	1.68	1.28
	PAW-LDA[a]	3.85		1.67	1.50
	PAW-LDA[b]	3.862	208		1.44
	PAW-PBE[b]	3.958	157		1.19
	PAW-AM05[b]	3.871	189		1.43
	LSGF-LDA			1.43[c]	
	FP-LMTO-LDA			1.65[d]	
	Exp.	3.891[e]	195[f]		1.85[g]
					1.7[h]
					1.5[h]
Ag	EMTO-LDA	4.015	137	1.20	1.05
	EMTO-AM05	4.067	114	1.16	1.03
	EMTO-PBE	4.160	90	0.86	0.76
	EMTO-PBEsol	4.066	115	1.15	0.88
	PAW-LDA[b]	4.027	106		1.03
	PAW-PBE[b]	4.169	86		0.78
	PAW-AM05[b]	4.058	126		1.00
	LSGF-LDA			0.99[c]	
	FP-LMTO-LDA			1.24[d]	
	Exp.	4.086[e]	104[f]		1.31[h]
					1.11[i]
					1.00[i]

projector augmented wave (PAW) method and experimental ones regardless the used xcf. Lattice parameter a shows a maximum 2% deviation compared to the available data.

Numerical difficulties in addressing the quantitative description of bulk modulus B within the Morse type of equation of state (EOS) yield larger disagreements. The largest deviation between the theoretical results for a given xcf is 7% for Pd (LDA) and 10% for Ag (LDA, PBE). This deviation may be accounted for by the difference between applied methods and EOS's. Comparing EMTO results with the experimental data the largest 14 (30) % deviation for B of Pd (Ag) obtained using LDA functional can be reduced to 2 (10) % using the recently developed AM05 approximation. Here we should recall that the present theoretical results were obtained at static conditions, whereas the experimental data refer to room temperature.

B. Vacancy formation energy of Pd and Ag

Volume-relaxed ($H_{\rm vr}$) and fully relaxed ($H_{\rm fr}$) vacancy formation energies of Pd and Ag calculated using the EMTO method are in good agreement with the former PAW results within LDA, AM05, and PBE formulations of the xcf and with full-potential linear muffin-tin orbital (FP-LMTO) LDA data, the largest difference being 5%. There are no former theoretical data calculated using the PBEsol functional. The locally self-consistent Green's-function (LSGF) LDA calculations give somewhat lower $H_{\rm vr}$ compared to the present and previous PAW and FP-LMTO simulations.

There is a large variation for the experimental $H_{\rm vac}$ of Pd. Positron annihilation spectroscopy (PAS) measurement gives 1.85 eV [59], while thermal conductivity and thermal diffusivity experiments report 1.7 and 1.5 eV, respectively [32]. In general, the theoretical $H_{\rm vr}$ obtained with the present EMTO and former DFT methods within the LDA and AM05 schemes are in very good agreement with the thermal conductivity data ($\pm$1%). These values are smaller with 7% than PAS results which is commonly regarded as the most accurate experimental tool. However, when local lattice relaxation is allowed in the DFT simulations, values for $H_{\rm fr}$ are lower with $\approx$20%. The discrepancy between the experimental and EMTO data is more accentuated for PBEsol/PBE (30/25%).

In the case of Ag, PAS reports 1.31 and 1.11 eV for $H_{\rm vac}$ depending on lifetime and mean lifetime measurements. Thermopower experiments give 1.00 eV. Theoretical $H_{\rm vr}$ ($H_{\rm fr}$) data obtained using LDA and AM05 are within 8 ($-$5) % compared to the recommended experimental value 1.11 eV [60].

The fact that the volume-relaxed vacancy formation energies ($H_{\rm vr}$) are closer to the experimental values maybe accidental. For a better description of the underlying physical phenomena the effect of the local lattice relaxation cannot be neglected. On one hand, the large discrepancy between $H_{\rm fr}$ and the experimental data may be accounted for by the performance of the different xcf's when they describe the internal free surface created by the introduced vacancy [33,34,36,38]. Due to the well known error-cancellation effects present in LDA, i.e., overestimation of the exchange energy of a free metal surface and underestimation of the correlation energy by approximately the same magnitude [61], LDA gives the most reasonable $H_{\rm fr}$ compared to the experimental data. In the case of the generalized gradient approximations (GGA) (PBEsol belongs to this group of xcf functionals) results are very dependent on the parametrization. PBEsol performs better than the Perdew-Burke-Ernzerhof GGA (PBE) [62] for $H_{\rm fr}$ with 5 (12) % for Pd (Ag) compared to the LDA values. Functional-dependent correction to the vacancy formation energies of pure metals has been proposed by several former theoretical studies [33,34,36,38]. Application of such additional correction schemes goes beyond the aim of the present study; moreover such a surface description correction is included by construction in the AM05 functional.

On the other hand, recent theoretical simulations show in the case of Cu and Al that nonlinear thermal corrections may be crucial when the high-temperature experimental data are extrapolated to 0 K [55,63,64], and therefore the 0 K theoretical values may not be directly comparable to the extrapolated experimental values. The temperature-dependent Gibbs energy of vacancy formation for Al and Cu was calculated considering all the relevant excitation mechanisms: electronic temperature effects, lattice vibrations within the quasiharmonic approximation, and phonon-phonon interactions (anharmonic lattice vibration effects). It was shown that the formation entropy of the vacancy is highly affected by the anharmonicity that results in a nonlinear temperature dependence of the vacancy formation energy. Including these corrections when the experimental data are extrapolated to 0 K, lower values for the vacancy formation energy of Al and Cu are derived [55]. The discrepancies between the PAS and differential dilatometry data are explained as well. Unfortunately, the correction of the extrapolated 0 K experimental data is impossible for Pd, Ag, and their alloys due to the lack of detailed measurements. Calculation of temperature-dependent vacancy formation energy is beyond the scope of this work. Nonetheless, the presented 0 K theoretical results may be considered an upper (LDA results) or lower (PBE results) bound for the experimental data [55,65].

C. Effective chemical potentials

The measure of the interaction between the alloy components and vacancy was investigated via the effective chemical potential (ECP) [21,43]. The ECPs calculated for the first coordination shell around the vacancy and the sixth coordination shell, the latter corresponding approximately to the bulk ECP, shed light on the ordering (short and long range ordering) or segregation tendencies in PdAg alloys with monovacancy. Three alloys with different composition were considered here, $Pd_{0.8}Ag_{0.2}$, $Pd_{0.5}Ag_{0.5}$, and $Pd_{0.2}Ag_{0.8}$. The Pd-Ag effective chemical potential was calculated according to

$$\Delta\mu^s_{\rm Pd-Ag} \equiv \mu^s_{\rm Pd} - \mu^s_{\rm Ag} = \frac{\partial E^s_{\rm SC}(n,c)}{\partial c} \approx \frac{E^s_{\rm SC}(n,c+\delta) - E_{\rm SC}(n,c)}{\delta}, \quad (1)$$

where $E_{\rm SC}(n,c)$ is the total energy of the 32-site supercell with a base composition on all atomic sites; $E^s_{\rm SC}(n,c+\delta)$ is the total energy of the supercell with δ concentration variation in the first ($s=1$) or sixth ($s=6$) coordination shell. In the present application we adopted $\delta = 0.01$. The effective chemical

potentials of Ag are $\Delta\mu^1_{\rm Ag} = -202.5342$ (-202.5270/-202.5117) and $\Delta\mu^6_{\rm Ag} = -202.5311$ (-202.5239/-202.5090) for $Pd_{0.8}Ag_{0.2}$ ($Pd_{0.5}Ag_{0.5}$/$Pd_{0.2}Ag_{0.8}$) in the case of the Pd-Ag exchange process. Accordingly, Ag atoms prefer positions around the vacancy while Pd prefers bulk positions (far away from the vacancy).

The "segregation energy" around the vacancy becomes $\Delta\mu^1_{\rm Ag} - \Delta\mu^6_{\rm Ag} = -3.1$, -3.1, and -2.7 mRy/atom for $Pd_{0.8}Ag_{0.2}$, $Pd_{0.5}Ag_{0.5}$, and $Pd_{0.2}Ag_{0.8}$, respectively. The configurational entropy opposes the Pd-Ag exchange process with increasing temperature and favors a more homogenous distribution around the vacancy. From the condition of vanishing $\Delta\mu^1_{\rm Ag}(T) - \Delta\mu^6_{\rm Ag}(T) \approx \Delta\mu^1_{\rm Ag} - \Delta\mu^6_{\rm Ag} + k_{\rm B}T\ln[c^1(1-c)/(1-c^1-c)]$, at temperature T, the equilibrium Ag concentration in the first coordination shell around the vacancy becomes

$$c^1 = \frac{c}{c + (1-c)e^{(\Delta\mu^1_{\rm Ag} - \Delta\mu^6_{\rm Ag})/k_{\rm B}T}}, \qquad (2)$$

where $k_{\rm B}$ is the Boltzmann constant. The Ag concentration around the vacancy at room temperature ($T = 300$ K) is estimated to be 0.56, 0.84, and 0.94 in the case of $Pd_{0.8}Ag_{0.2}$, $Pd_{0.5}Ag_{0.5}$, and $Pd_{0.2}Ag_{0.8}$, respectively, indicating a high tendency for segregation. On the other hand, at temperatures close to the melting point of these alloys, where the vacancy formation energy is measured, c^1 of Ag becomes only 6 ± 2 % higher than its bulk value. This low deviation for the high-temperature Ag concentration around the vacancy from its bulk value indicates that segregation is not likely in these systems at high temperature. A possible short-range ordering may appear. Investigations of the short-range order (SRO) effects published by Hoffmann *et al.* [27] show that at 0 K SRO results are in substantial agreement with the data calculated within the fully random distribution framework of CPA. These theoretical findings supports the validity of the present study performed on homogenous alloys.

D. Bulk properties of $Pd_{1-x}Ag_x$ alloys in the presence of monovacancy

Bulk parameters and $H_{\rm vac}$ of pure Pd and Ag calculated with EMTO agreed well with the previous theoretical data giving us confidence to proceed to evaluation of those parameters for $Pd_{1-x}Ag_x$ as a function of Ag content. Composition-dependent bulk parameters (a, B) of $Pd_{1-x}Ag_x$ alloys calculated for perfect (fcc) and defected (SC) crystal structure are listed in Table II. Data for fcc alloys are identical to ones presented in Ref. [25]. For a detailed discussion of the composition-dependent a and B of fcc $Pd_{1-x}Ag_x$ alloys the reader is directed to Ref. [25].

Volume relaxation due to the 1/32 vacancy concentration is only 0.3 ± 0.1 % over the whole concentration range regardless of the used xcf. Similar negligible volume change has been found by former theoretical studies conducted on simple metals [35,38]. Softening of the defected crystal structure against hydrostatic pressure, e.g., decrease of B, is about 4%. High deviation from the linear composition dependence of

TABLE II. Theoretical lattice parameters (Å), bulk modulus (GPa) for fcc and supercell (SC) Pd-Ag alloys, volume-relaxed ($H_{\rm vr}$) and fully relaxed ($H_{\rm fr}$) vacancy formation energies (eV), the equilibrium local relaxation η_0 (%) calculated within LDA, and AM05, PBEsol, and PBE form of the exchange-correlation functional for $Pd_{1-x}Ag_x$ (x in at. %).

	LDA							AM05						
x	$a^{\rm fcc}$	$B^{\rm fcc}$	$a^{\rm SC}$	$B^{\rm SC}$	$H_{\rm vr}$	$H_{\rm fr}$	η_0	$a^{\rm fcc}$	$B^{\rm fcc}$	$a^{\rm SC}$	$B^{\rm SC}$	$H_{\rm vr}$	$H_{\rm fr}$	η_0
0	3.854	223	3.843	213	1.72	1.48	−1.33	3.884	199	3.874	190	1.72	1.50	−1.30
10	3.869	212	3.858	204	1.72	1.49	−1.30	3.900	189	3.891	181	1.71	1.51	−1.28
20	3.883	202	3.873	194	1.66	1.45	−1.28	3.918	178	3.908	171	1.64	1.45	−1.26
30	3.898	192	3.888	185	1.61	1.41	−1.26	3.934	169	3.925	162	1.58	1.41	−1.24
40	3.914	184	3.903	177	1.59	1.40	−1.25	3.951	160	3.942	154	1.55	1.39	−1.22
50	3.929	175	3.919	169	1.56	1.39	−1.22	3.969	152	3.960	145	1.52	1.37	−1.20
60	3.945	167	3.934	161	1.43	1.26	−1.23	3.987	143	3.977	138	1.39	1.25	−1.21
70	3.959	159	3.950	153	1.36	1.20	−1.25	4.004	135	3.996	130	1.31	1.17	−1.21
80	3.977	152	3.967	146	1.31	1.15	−1.26	4.024	129	4.016	123	1.26	1.12	−1.22
90	3.997	142	3.985	139	1.11	0.95	−1.29	4.047	118	4.036	116	1.08	0.95	−1.25
100	4.015	137	4.004	131	1.20	1.05	−1.31	4.067	114	4.058	108	1.16	1.03	−1.27
	PBEsol							PBE						
x	$a^{\rm fcc}$	$B^{\rm fcc}$	$a^{\rm SC}$	$B^{\rm SC}$	$H_{\rm vr}$	$H_{\rm fr}$	η_0	$a^{\rm fcc}$	$B^{\rm fcc}$	$a^{\rm SC}$	$B^{\rm SC}$	$H_{\rm vr}$	$H_{\rm fr}$	η_0
0	3.889	205	3.879	192	1.68	1.28	−1.52	3.956	165	3.946	159	1.38	1.21	−1.25
10	3.906	192	3.895	183	1.67	1.30	−1.51	3.975	156	3.965	150	1.38	1.22	−1.24
20	3.922	180	3.912	174	1.60	1.26	−1.50	3.994	147	3.984	142	1.31	1.17	−1.21
30	3.938	170	3.928	165	1.55	1.23	−1.46	4.013	139	4.003	134	1.25	1.12	−1.18
40	3.955	161	3.945	157	1.53	1.22	−1.44	4.032	131	4.022	126	1.22	1.10	−1.16
50	3.972	152	3.962	149	1.50	1.22	−1.44	4.051	124	4.042	119	1.21	1.10	−1.13
60	3.989	143	3.979	142	1.37	1.10	−1.44	4.072	116	4.061	112	1.10	1.00	−1.14
70	4.006	136	3.997	134	1.29	1.03	−1.46	4.091	109	4.082	106	1.00	0.89	−1.14
80	4.025	128	4.016	127	1.24	0.99	−1.47	4.112	104	4.104	99	0.95	0.84	−1.17
90	4.047	121	4.036	120	1.07	0.81	−1.50	4.140	93	4.127	93	0.85	0.74	−1.20
100	4.066	115	4.057	112	1.15	0.88	−1.52	4.160	90	4.152	85	0.86	0.76	−1.21

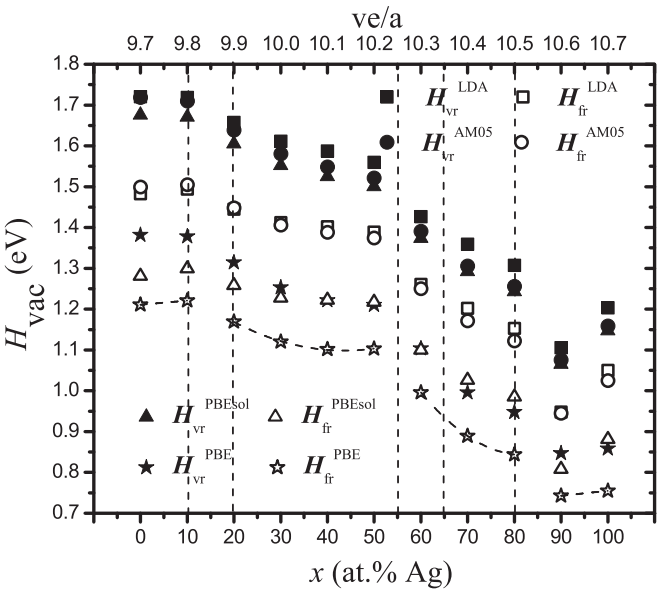

FIG. 1. Vacancy formation energy H_{vac} for fcc $Pd_{1-x}Ag_x$ as a function of composition (bottom axis) and valance electron per atom (top axis) calculated for four different exchange-correlation functionals: LDA (squares), AM05 (circles), PBEsol (triangles), and PBE (stars). Volume-relaxed values are labeled by filled symbols, and open symbols stand for the fully relaxed vacancy formation energy. Vertical dashed-dotted lines mark the positions of FSTT's.

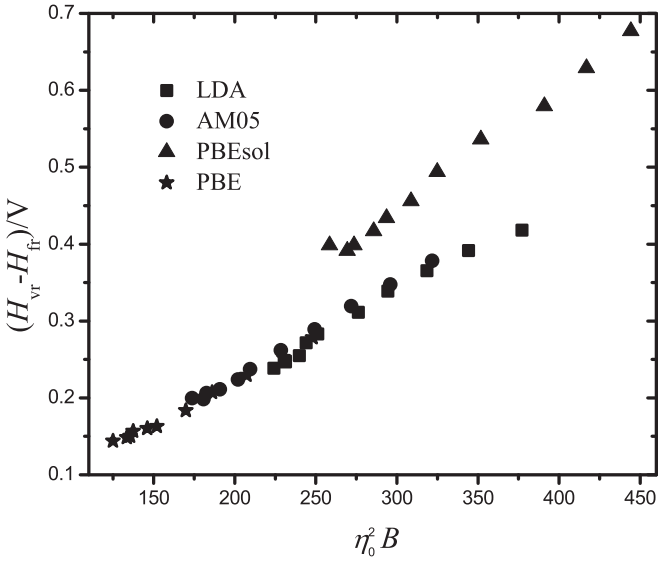

FIG. 2. Linear correlation between $(H_{vr} - H_{fr})/V$ and $\eta_0^2 B$.

the lattice parameter and bulk modulus of the defected crystal (not shown) is found similarly to the case of perfect crystals. Previous theoretical studies [16,25,27] discuss in detail the relation between such anomalies and Fermi surface topological transitions.

E. Local relaxation effects on the vacancy formation energy

Monovacancy formation energies calculated for $Pd_{1-x}Ag_x$ alloys are listed in Table II and plotted in Fig. 1 as a function of Ag concentration and different xcf's. For H_{vr}, three out of four xcf's give very similar values to each other: AM05 (PBEsol) values are on average 0.03 ± 0.03 (0.06 ± 0.01) eV lower than the LDA values throughout the Ag concentration range. In general, PBE gives 23% lower values than LDA.

Local relaxation effects on the vacancy formation energy have similar magnitude for LDA, AM05, and PBE. Values decrease by 12 ± 1 % for LDA and 11 ± 2 % for AM05 (PBE). The relaxation effects in the case of PBEsol are more pronounced, by about 20 ± 2 %. This observation may be explained by investigating the equilibrium local relaxation values (η_0) listed in Table II. The η_0 values are similar for LDA, AM05, and PBE functionals. An average value is -1.275 ± 0.055 % and -1.25 ± 0.05 % for LDA and AM05, respectively, throughout the Ag concentration range. PBE shows the lowest average value for η_0, e.g., -1.19 ± 0.06 %. The average η_0 is much higher for the PBEsol functional, namely -1.48 ± 0.04 %. The larger local relaxation in the case of PBEsol leads to a lower H_{fr} value than for H_{fr}^{AM05}. The linear correlation between $(H_{vr} - H_{fr})/V$ and $\eta_0^2 B$ presented in Fig. 2 still holds for PBEsol as well as for other functionals, but we can find a shift in the case of PBEsol compared to the other functionals due to larger η_0 and the induced energy difference.

Here we would like to point out that for all functionals considered here, the size of the local lattice relaxation shows weak composition dependence. We may conclude that the local relaxation is not sensitive to the chemical environment. This finding supports our assumption that the local lattice relaxation can be reasonably well captured within the present mean-field approximation.

F. Composition-dependent monovacancy formation energy of $Pd_{1-x}Ag_x$ alloys

We find a nonlinear composition dependence of H_{vr} and H_{fr} presented in Fig. 1. The calculated data points are grouped in order to highlight this strong nonlinear behavior and the abrupt changes in the composition dependence of the theoretically estimated H_{vr} and H_{fr}. The grouping is shown only for H_{fr} calculated with PBE together with the position of FSTT. Previous theoretical works [16,25,29] show that the nonlinear composition dependence of some physical parameters (lattice parameters, elastic constants, surface energies) may be associated with the abrupt change in the FS topology. For example the largest deviation from the linear behavior in the case of the $Pd_{1-x}Ag_x$ lattice parameter occurs at the equiatomic concentration [25], where the ellipsoid hole pocket centered at X disappears. A relation between the positions of the anomalies and the critical concentrations of FSTT can be detected in the case of $H_{vac}(x)$ as well.

IV. DISCUSSION

A. Local relaxation and the exchange-correlation functionals

According to the η_0 values listed in Table II, LDA, AM05, PBEsol, and PBE functionals lead to different magnitude of local relaxation for the first neighboring shell around the vacancy. We notice that the AM05 and PBE relaxations are rather close to the LDA relaxations. On average throughout the

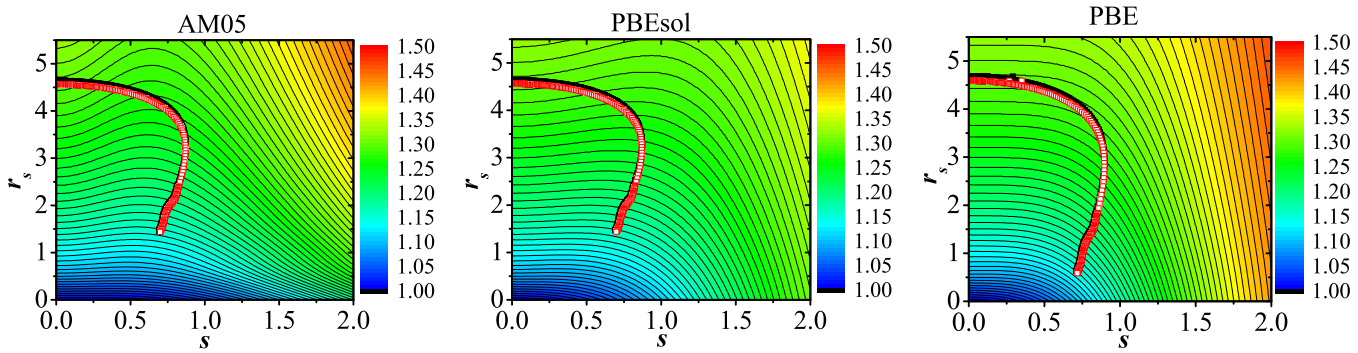

FIG. 3. (Color online) Contour plot of the $F_{xc}(s,r_s)$ enhancement function generated for AM05, PBEsol, and PBE exchange correlation functionals. Black (red) line stands for $r_s(s)$ values calculated around the vacancy in the volume-relaxed (fully relaxed) Pd supercell.

Ag concentration range, when LDA (AM05/PBE) is used to calculate η_0 and H_{fr}, atoms in the first neighboring shell move closer to the vacancy by -1.275 ± 0.055 % (-1.25 ± 0.05/ -1.19 ± 0.06 %) while PBEsol allows for -1.48 ± 0.04 % local relaxation. The difference between AM05, PBEsol, and PBE functionals with respect to LDA may be investigated by analyzing the so called enhancement function $F_{xc}(s,r_s)$ defined as follows:

$$F_{xc}(s,r_s) \approxeq F_{xc}[n] = \epsilon_{xc}[n]/\epsilon_x^{LDA}(n), \quad (3)$$

where n is the electronic density, $\epsilon[n]$ is the exchange-correlation density per electron for a certain approximation, and $\epsilon_x^{LDA}(n)$ is the LDA exchange energy density per electron. Within the gradient-level approximation, the density dependence of the exchange-correlation energy functional is represented by a function that depends on the scaled gradient s and the electronic Wigner-Seitz radius r_s. For further details the reader is referred to Ref. [66]. Here, we present the enhancement function for AM05, PBEsol, and PBE in Fig. 3 as a function of s and r_s, and with the characteristic s and r_s values of Pd. We notice that for LDA, F_{xc} is obtained from Fig. 3 at $s = 0$. The black $r_s(s)$ curve corresponds to the volume-relaxed values and the $r_s(s)$ values for the fully relaxed supercell are represented by the red line. During the relaxation, the atoms move closer to the vacant site decreasing the inner surface around the vacant atom that leads to an increase in the electron density. This is represented by a small shift of r_s towards smaller values in low and middle s range (0–0.7), while s values decrease in $1.5 \leqslant r_s \leqslant 3$. The change of the $r_s(s)$ curve due to the relaxation happens in that region where the difference between $F_{xc}(s,r_s)$ of AM05, PBEsol, and PBE is considerable. In case of AM05, $r_s(s)$ moves towards a local $F_{xc}(s,r_s)$ minimum, as a consequence the contribution of the exchange energy (which is negative) to the total energy decreases for lager relaxation. The opposite happens in the case of PBEsol. Due to the relaxation, $r_s(s)$ moves out from the local $F_{xc}(s,r_s)$ minimum contributing with a larger amount of exchange energy to the total energy. As a consequence, PBEsol allows for larger relaxation as compared to AM05. Moreover, in the interesting s-r_s region $F_{xc}(s,r_s)$ is a more rapidly varying function for PBEsol than for AM05 and PBE (see Fig. 3). The behavior of $r_s(s)$ in the case of PBE is similar to AM05, but the change in $F_{xc}(s,r_s)$ is shallower, which leads to the lower η_0 for PBE than for AM05. Similar behavior is found for Ag as well (not shown). Therefore, the additional effects introduced via $F_{xc}(s,r_s)$ for AM05, PBE, and PBEsol with respect to LDA and the delicate differences between AM05, PBEsol, and PBE functionals turned out to be significant when describing vacancies. The rapid change in $F_{xc}(s,r_s)$ in the case of PBEsol compared to the shallower $F_{xc}(s,r_s)$ for the other two functionals leads to additional effects compared to AM05, PBE, and LDA. These features are nicely reflected by the predicted local lattice relaxations around the point defect and the corresponding change in the vacancy formation energy.

B. Electronic structure and Fermi surface of $Pd_{1-x}Ag_x$ alloys

Densities of states of pure fcc Pd and Ag are presented in Fig. 4. The Fermi energy of pure Pd lies within the d band, while for Ag it is located in the sp band. As a consequence Pd has a complex Fermi surface, while the Fermi surface of Ag is noble-metal-like. The intersections of Fermi surfaces (FS) of the pure elements with the ΓKLUX plane calculated using the scalar-relativistic EMTO-CPA method are depicted in Fig. 5. The following parts of the Pd FS have been identified:

(1) an octahedron electron pocket (closed surface) centered at the Γ point with sp character,

(2) an ellipsoid hole pocket centered at the X point having d character, and

(3) a hole jungle-gym structure (open surface) which is connected at the point L, also having d character.

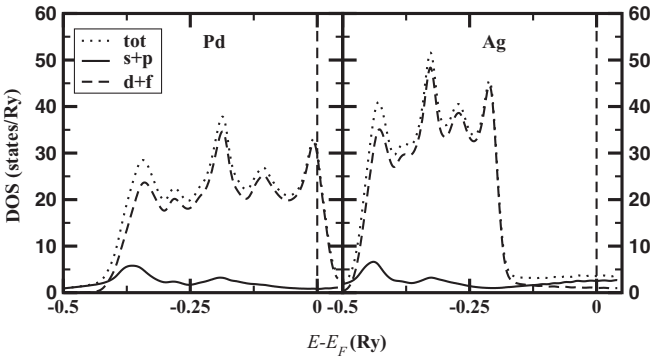

FIG. 4. Density of states of pure fcc Pd and Ag. Fermi energy is set to 0.

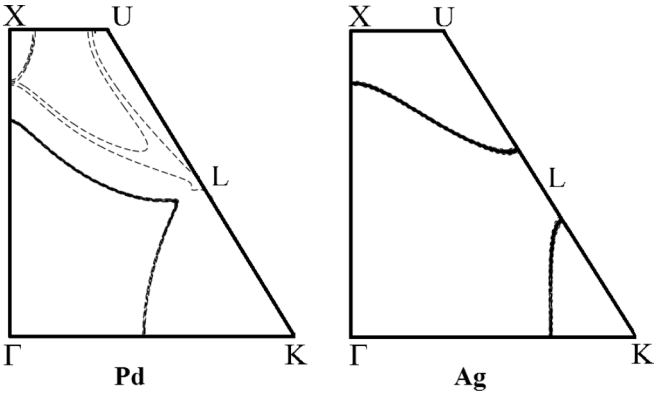

FIG. 5. Fermi surface of pure fcc Pd and Ag. Full line stand for the electron surfaces and dashed line for the hole surfaces.

The presented FS for Pd is in agreement with the former theoretical results [16,67]. The connection of the jungle-gym structures at L was not detected in the earlier work of Andersen [67], but it has been shown by Bruno *et al.* [16]. The structure of the Pd FS was confirmed experimentally by de Haas–van Alphen spectroscopy [68–73]. The Ag FS is noble-metal-like with an octahedron electron pocket centered at the Γ with broken necks at L and a belly centered at Γ lying on the Γ-X line. Galvanomagnetic measurements [74] and de Haas–van Alphen spectroscopy [75,76] corroborate the theoretical finding.

Doping Pd with Ag, i.e., electron addition, brings the FS from a complex structure typical for Pd to a more simple noble-metal-like FS. A few percent of Ag addition first fills the hole pockets, then at higher Ag content a neck will appear at the L point. These changes in the FS topology may arise continuously or suddenly. The evolution of the $Pd_{1-x}Ag_x$ FS is presented in Fig. 6 for some concentrations. The concentration change when doping Ag into Pd is similar with the increase of the number of valence electrons per atoms (ve/a). Already 10 at. % Ag (10.1 ve/a) addition induces changes in the jungle-gym hole pockets at L (1st transition). At 20 at. % of Ag (10.2 ve/a) the jungle-gym hole structure completely disappears (2nd transition). One can observe that there is already one single hole pocket at X, which still exists at $x = 0.5$ (10.5 ve/a) but suddenly disappears at $x = 0.55$ (10.55 ve/a) (3rd transition). At 65 at. % of Ag (10.65 ve/a) the neck centered at L is touching the Brillouin zone (4th transition) and becomes completely open at $x = 0.8$ (10.8 ve/a) (5th transition). The changes in the FS topology detected with the present theoretical methodology are in good agreement with the previous theoretical findings by Bruno *et al.* [16]. The critical concentrations given by Ref. [16] are 0.06, 0.20, 0.35, 0.53, and 0.70. There are no experimental data for alloys to compare the theoretical results with.

The energetics of such a transition in the FS topology may be understood in connection with the partial pressure of the different bends and their effect on the EOS, discussed in general by Pettifor [77] and in relation to PdAg alloys by Ref. [25].

Figure 1 shows three abrupt changes in the composition dependence of H_{vac}. They occur between 20–30, 50–60, and 80–90 at. % Ag. Although the direct energetical relation

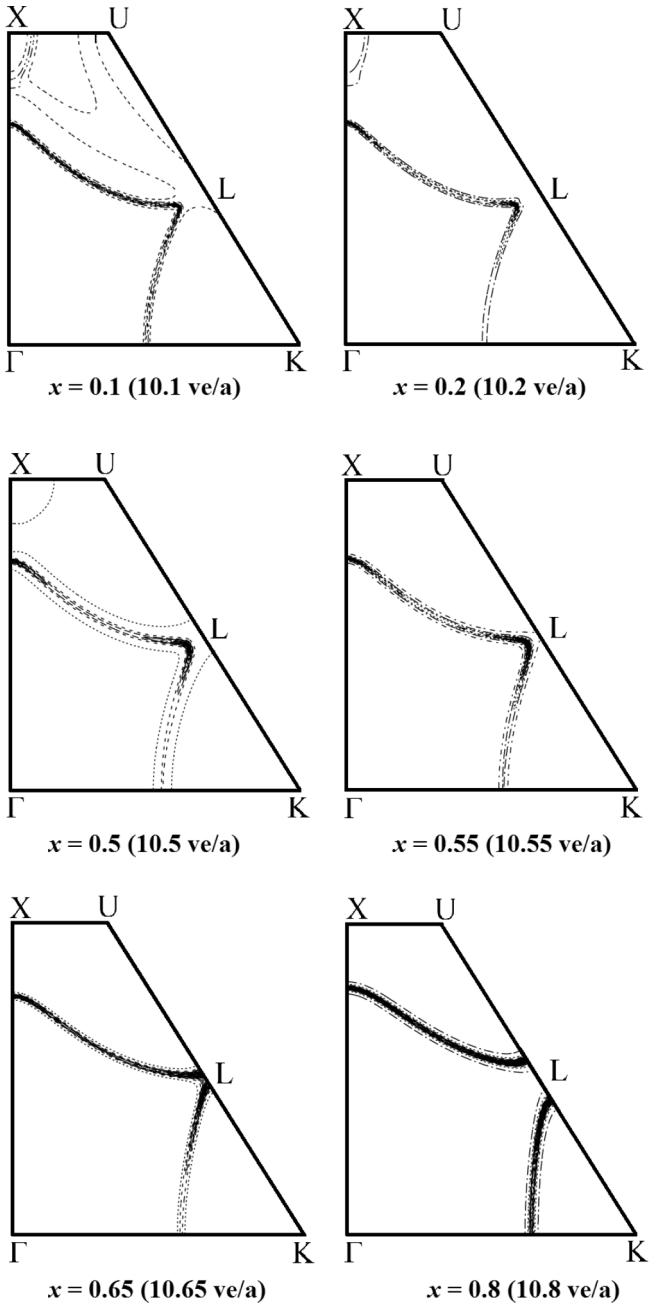

FIG. 6. Fermi surface of fcc $Pd_{1-x}Ag_x$.

between vacancy formation and a transition in FS topology is not known, we find a good correspondence between the abrupt changes in the composition-dependent H_{vac} and the critical concentrations for FSTT marked by vertical dashed-dotted lines in Fig. 1. The nonlinear composition dependence of H_{vac} may be a consequence of a direct relation between vacancy and FS as well as the indirect effect of FSST on the composition-dependent EOS since anomalous behavior for lattice parameters of defected cells is present as well as for the bulk fcc alloys.

Moreover, the effect of vacancy in the Fermi surface has to be taken into account when $H_{vac}(x)$ is related to FSTT's. Introducing a vacant site to the fcc system means electron removal. The appearance of a FSTT is related to the number

of valance electrons per atom, not to the actual concentration of Ag in $Pd_{1-x}Ag_x$ alloys. Therefore, we expect an overlap and superposition of between different FSTT's in the case of supercells. This could lead as well to a shift in the concentration where the transition takes place. For instance, there is an abrupt change in $H_{vac}(x)$ for $0.8 < x < 0.9$. According to Fig. 6 FSTT is already finished at $x = 0.8$ in the case of fcc alloy and no more topological transition occurs with increasing Ag content. But in the case of supercells, the ve/a is shifted to 10.5–10.6 for $0.8 < x < 0.9$, where actually a hole pocket centered at X disappears. The effect of the 4th transition may also play a role here. We believe that the superposition of the 3rd, 4th, and 5th FSTT is responsible for the sudden change in $H_{vac}(x)$ for $x \approx 0.9$.

V. CONCLUSIONS

Vacancy formation energies for $Pd_{1-x}Ag_x$ alloys have been calculated with the EMTO method using four different exchange-correlation functionals, LDA, AM05, PBEsol, and PBE. We show that with the applied theoretical methodology we are able to reproduce the previously obtained theoretical values for the volume and structural relaxed vacancy formation energies of Pd and Ag with LDA and AM05 xcf's. Completely new data are presented for the end points using the PBEsol functional, and for the alloys. Hereby we call the experimentalist for a more detailed study of this technologically important alloy.

We also found that the local relaxation effects have a big impact on the $H_{vac}(x)$ values and are very much dependent on the used exchange-correlation functionals. Nevertheless, the composition dependence of the local lattice relaxation is rather weak for all approximations employed here supporting that the present mean-field approximation is appropriate to describe this effect. AM05 (PBE) allows for lower local relaxation than PBEsol due to different behavior of the enhancement function in the region scanned by $r_s(s)$. This will lead to about 8% smaller H_{fr} values obtained by PBEsol than AM05. The difference between H_{fr} values calculated with PBE and other functionals becomes smaller compared to H_{vr} values, due to the smaller magnitude for lattice relaxation in the case of PBE.

Both H_{vr} and H_{fr} are presented for $Pd_{1-x}Ag_x$ for the whole Ag concentration range. We find nonlinear dependence of $H_{vac}(x)$ on the Ag content with abrupt changes between 20–30, 50–60, and 80–90 at. % Ag, respectively. The Fermi surface of Pd and Ag are presented in detail. Changes in the Fermi surface topology due to the electron addition, i.e., increasing Ag content, are discussed and they are related to the nonlinear composition dependence of H_{vac}.

ACKNOWLEDGMENTS

The European Research Council, the Swedish Research Council, and the Swedish Foundation for Strategic Research are acknowledged for financial support. O.E. acknowledges support from eSSENCE, STandUP, and the KAW foundation. The Hungarian Scientific Research Fund (research project OTKA 84078 and 109570) is acknowledged for financial support (L.V.). Calculations were performed on UPPMAX and C3SE resources.

[1] R. L. Bertolotti, in W. J. O'Brien, editor, *Dental Materials and Their Selection*, 3rd edition (Quintessence, Chicago, 2002), Chap. 14; P. R. Mezger, A. L. H. Stols, M. M. A. Vrijhoef, and E. H. Greener, J. Dent. **17**, 90 (1989); E. Papazoglou and W. A. Brantley, Dent. Mater. **14**, 112 (1998); T. R. Walton and W. J. O'Brien, J. Dent. Res. **64**, 476 (1985); P. R. Mezger, M. M. A. Vrijhoef, and E. H. Greener, Dent. Mater. **5**, 97 (1989).

[2] L. Joska, M. Marek, and J. Leitner, Biomaterials **26**, 1605 (2005).

[3] H. Wang, Y. Zhang, H. Li, B. Du, H. Ma, D. Wu, and Q. Wei, Biosens. Bioelectron. **49**, 14 (2013).

[4] M. Wang and Y. Feng, Sens. Actuators B **123**, 101 (2007).

[5] J. C. Dellamorte, J. Lauterbach, and M. A. Barteau, Appl. Cat. A: Gen. **391**, 281 (2011).

[6] F. A. Lewis, J. P. Magennis, S. G. McKee, and P. J. M. Ssebuwufu, Nature (London) **306**, 673 (1983).

[7] H. D. Tong, F. C. Gielens, J. G. E. Gardeniers, H. V. Jansen, J. W. Berenschot, M. J. de Boer, J. H. de Boer, C. J. M. van Rijn, and M. C. Elwenspoek, J. Microelectromech. Syst. **14**, 113 (2005).

[8] L. W. McKeehan, Phys. Rev. **20**, 424 (1922).

[9] *Binary Alloy Phase Diagrams*, edited by T. B. Massalski (ASM International, Metals Park, OH, 1992).

[10] I. Coulthard and T. K. Sham, Phys. Rev. Lett. **77**, 4824 (1996).

[11] S. K. Parida, V. R. R. Medicherla, P. Bag, R. Rawat, T. Shripathi, N. Dahadev, S. Thakur, D. Biswas, G. Adhikay, and K. Maiti, Mat. Res. Exp. **1**, 046501 (2014).

[12] B. R. Coles, J. Inst. Met. **84**, 346 (1956); W. B. Pearson, *A Handbook of Lattice Spacings and Structures of Metals and Alloys* (Pergamon press, New York, 1958), p. 298.

[13] A. Gonis, W. H. Butler, and G. M. Stocks, Phys. Rev. Lett. **50**, 1482 (1983).

[14] S. Takizawa, K. Terakura, and T. Mohri, Phys. Rev. B **39**, 5792 (1989).

[15] I. A. Abrikosov and H. L. Skriver, Phys. Rev. B **47**, 16532 (1993).

[16] E. Bruno, B. Ginatempo, and E. S. Giuliano, Phys. Rev. B **52**, 14544 (1995); **52**, 14557 (1995).

[17] K. Kokko, R. Laihia, M. Alatalo, P. T. Salo, M. P. J. Punkkinen, I. J. Väyrynen, W. Hergert, and D. Ködderitzsch, Phy. Rev. B **60**, 4659 (1999).

[18] S. Müller and A. Zunger, Phys. Rev. Lett. **87**, 165502 (2001).

[19] S. Pella, J. S. Faulkner, G. M. Stocks, and B. Ujfalussy, Phys. Rev. B **70**, 064203 (2004).

[20] H. H. Kart, M. Tomak, M. Uludoğan, and T. Čağin, Comput. Mater. Sci. **32**, 107 (2005).

[21] M. Ropo, K. Kokko, L. Vitos, J. Kollár, and B. Johansson, Surf. Sci. **600**, 904 (2006).

[22] A. V. Ruban, S. I. Simak, P. A. Korzhavyi, and B. Johansson, Phys. Rev B **75**, 054113 (2007).

[23] K. Kokko, M. Ropo, M. P. J. Punkkinen, P. Laukkanen, M. Alatalo, L. Vitos, J. Kollár, and B. Johansson, Surf. Sci. **601**, 5419 (2007).

[24] L. Vitos, M. Ropo, K. Kokko, M. P. J. Punkkinen, J. Kollár, and B. Johansson, Phys. Rev. B **77**, 121401(R) (2008).

[25] E. K. Delczeg-Czirjak, L. Delczeg, M. Ropo, K. Kokko, M. P. J. Punkkinen, B. Johansson, and L. Vitos, Phys. Rev. B **79**, 085107 (2009).

[26] E. K. Delczeg-Czirjak, E. Nurmi, K. Kokko, and L. Vitos, Phys. Rev. B **84**, 094205 (2011).

[27] M. Hoffmann, A. Marmodoro, E. Nurmi, K. Kokko, L. Vitos, A. Ernst, and W. Hergert, Phys. Rev. B **86**, 094106 (2012).

[28] Fu-Yang Tian, Nan-Xian Chen, L. Delczeg, and L. Vitos, Comput. Mater. Sci. **63**, 20 (2012).

[29] Song Lu, Qing-Miao Hu, E. K. Delczeg-Czirjak, B. Johansson, and L. Vitos, Acta Mater. **60**, 4506 (2012).

[30] O. Yu. Vekilova, D. I. Bazhanov, S. I. Simak, and I. A. Abrikosov, Phys. Rev. B **80**, 024101 (2009).

[31] H. Kurokawa, K. Bada, M. Koyoma, M. Kubo, and A. Miyamoto, Appl. Surf. Sci. **244**, 636 (2005).

[32] Y. Kraftmakher, Phys. Rep. **299**, 79 (1998).

[33] K. Carling, G. Wahnström, T. R. Mattsson, A. E. Mattsson, N. Sandberg, and G. Grimvall, Phys. Rev. Lett. **85**, 3862 (2000).

[34] T. R. Mattsson and A. E. Mattsson, Phys. Rev. B **66**, 214110 (2002).

[35] R. Armiento and A. E. Mattsson, Phys. Rev. B **72**, 085108 (2005).

[36] A. E. Mattsson, R. Armiento, P. A. Schultz, and T. R. Mattsson, Phys. Rev. B **73**, 195123 (2006).

[37] L. Delczeg, E. K. Delczeg-Czirjak, B. Johansson, and L. Vitos, Phys. Rev. B **80**, 205121 (2009).

[38] R. Nazarov, T. Hickel, and J. Neugebauer, Phys. Rev. B **85**, 144118 (2012).

[39] C. Freysoldt, B. Grabowski, T. Hickel, J. Neugebauer, G. Kresse, A. Janotti, and C. G. Van de Walle, Rev. Mod. Phys. **86**, 253 (2014).

[40] T. Korhonen, M. J. Puska, and R. M. Nieminen, Phys. Rev. B **51**, 9526 (1995).

[41] P. A. Korzhavyi, I. A. Abrikosov, B. Johansson, A. V. Ruban, and H. L. Skriver, Phys. Rev. B **59**, 11693 (1999).

[42] L. Vitos, The EMTO Method and Applications, in *Computational Quantum Mechanics for Materials Engineers* (Springer-Verlag, London, 2007).

[43] L. Delczeg, B. Johansson, and L. Vitos, Phys. Rev. B **85**, 174101 (2012).

[44] P. Hohenberg and W. Kohn, Phys. Rev. **136**, B864 (1964).

[45] W. Kohn and L. J. Sham, Phys. Rev. **140**, A1133 (1965).

[46] L. Vitos, Phys. Rev. B **64**, 014107 (2001).

[47] O. K. Andersen, O. Jepsen, and G. Krier, in *Lectures on Methods of Electronic Structure Calculation* (World Scientific, Singapore, 1994), p. 63.

[48] L. Vitos, H. L. Skriver, B. Johansson, and J. Kollár, Comput. Mater. Sci. **18**, 24 (2000).

[49] J. Kollár, L. Vitos, and H. L. Skriver, in *Electronic Structure and Physical Properties of Solids: The Uses of the LMTO Method*, edited by H. Dreyssé, Lecture Notes in Physics (Springer-Verlag, Berlin, 2000), p. 85.

[50] P. Soven, Phys. Rev. **156**, 809 (1967).

[51] B. L. Gyorffy, Phys. Rev. B **5**, 2382 (1972).

[52] A. V. Ruban and H. L. Skriver, Phys. Rev. B **66**, 024201 (2002); P. A. Korzhavyi, A. V. Ruban, I. A. Abrikosov, and H. L. Skriver, *ibid.* **51**, 5773 (1995).

[53] J. P. Perdew and Y. Wang, Phys. Rev. B **45**, 13244 (1992).

[54] J. P. Perdew, A. Ruzsinszky, G. I. Csonka, O. A. Vydrov, G. E. Scuseria, L. A. Constantin, X. Zhou, and K. Burke, Phys. Rev. Lett **100**, 136406 (2008).

[55] A. Glensk, B. Grabowski, T. Hickel, and J. Neugebauer, Phys. Rev. X **4**, 011018 (2014).

[56] N. Chetty, M. Weinert, T. S. Rahman, and J. W. Davenport, Phys. Rev. B **52**, 6313 (1995).

[57] P. Ehrhart, P. Jung, H. Schultz, and H. Ullmaier, *Atomic Defects in Metals* (Springer-Verlag, Berlin, 1991).

[58] M. A. Shtremel, *Strength of Alloys*, Part 1. Lattice Defects (MISIS, Moscow, 1999).

[59] P. Ehrhart, in *Atomic Defects in Metals*, edited by H. Ullmaier, The Landolt-Börnstein-Database, III, Condensed Matter Vol. 25 (Springer-Verlag, Berlin, Heidelberg, 1991), http://materials.springer.com/lb/docs/sm_lbs_978-3-540-48128-7_65.

[60] P. Ehrhart, in *Atomic Defects in Metals*, edited by H. Ullmaier, The Landolt-Börnstein Database, III, Condensed Matter Vol. 25 (Springer-Verlag, Berlin, Heidelberg, 1991), http://materials.springer.com/lb/docs/sm_lbs_978-3-540-48128-7_57.

[61] S. Kurth, J. P. Perdew, and P. Blaha, Int. J. Quantum Chem. **75**, 889 (1999).

[62] J. P. Perdew, K. Burke, and M. Ernzerhof, Phys. Rev. Lett. **77**, 3865 (1996).

[63] B. Grabowski, L. Ismer, T. Hickel, and J. Neugebauer, Phys. Rev. B **79**, 134106 (2009).

[64] B. Grabowski, T. Hickel, and J. Neugebauer, Phys. Status Solidi B **248**, 1295 (2011).

[65] B. Grabowski, T. Hickel, and J. Neugebauer, Phys. Rev. B **76**, 024309 (2007).

[66] L. Delczeg, E. K. Delczeg-Czirjak, B. Johansson, and L. Vitos, J. Phys.: Condens. Matter **23**, 045006 (2011).

[67] O. K. Andersen, Phys. Rev B **2**, 883 (1970).

[68] J. J. Vuillemin and M. G. Prieetley, Phys. Rev. Lett. **14**, 307 (1965); J. J. Vuillemin, Phys. Rev. **144**, 396 (1966).

[69] L. R. Windmiller, J. B. Ketterson, and S. Hörnfeldt, Phys. Rev. B **3**, 4213 (1971).

[70] G. W. Crabtree, D. H. Dye, and D. P. Karim, J. Magn. Magn. Mater. **11**, 236 (1979).

[71] D. H. Dye, S. A. Campbell, G. W. Crabtree, J. B. Ketterson, N. B. Sandesara, and J. J. Vuillemin, Phys. Rev. B **23**, 462 (1981).

[72] C. Cavalloni, W. Joss, R. Monnier, and T. Jarlborg, Phys. Rev. B **31**, 1744 (1985).

[73] H. Ohlsén, P. Gustafsson, L. Nordborg, and S. P. Hörnfeldt, Phys. Rev. B **29**, 3022 (1984); H. Ohlsén, P. Gustafsson, and L. Nordborg, J. Phys. F: Met. Phys. **16**, 1681 (1986).

[74] N. E. Alekseevskii and Y. P. Gaidukov, J. Exptl. Theoret. Phys. **42**, 69 (1962) [Sov. Phys. JETP **15**, 49 (1962)].

[75] D. Shoenberg, Phil. Trans. A **255**, 85 (1962).

[76] M. R. Halse, Phil. Trans. A **265**, 507 (1969).

[77] D. G. Pettifor, J. Phys. F: Met. Phys. **8**, 219 (1978).